Accommodating Discontinuities in Dimeric Left-Handed Coiled Coils in ATP Synthase External Stalks

John G. Wise* and Pia D. Vogel
Department of Biological Sciences, Southern Methodist University, Dallas, Texas 75275

ABSTRACT ATP synthases from coupling membranes are complex rotary motors that convert the energy of proton gradients across coupling membranes into the chemical potential of the β-γ anhydride bond of ATP. Proton movement within the ring of *c* subunits localized in the F_0-sector drives γ and ε rotation within the F_1 $\alpha_3\beta_3$ catalytic core where substrates are bound and products are released. An external stalk composed of homodimeric subunits b_2 in *Escherichia coli* or heterodimeric *bb′* in photosynthetic synthases connects F_0 subunit *a* with F_1 subunits δ and most likely α. The external stalk resists rotation, and is of interest both functionally and structurally. Hypotheses that the external stalk contributes to the overall efficiency of the reaction through elastic coupling of rotational substeps, and that stalks form staggered, right-handed coiled coils, are investigated here. We report on different structures that accommodate heptad discontinuities with either local or global underwinding. Analyses of the knob-and-hole packing of the *E. coli* b_2 and *Synechocystis bb′* stalks strongly support the possibility that these proteins can adopt conventional left-handed coiled coils.

INTRODUCTION

The F_1F_0 ATP-synthase is a ubiquitous membrane-bound energy transformer that converts the electrochemical energy of proton gradients across coupling membranes into the chemical energy inherent in the condensation of ADP and P_i to ATP (1,2). The overall complexity of ATP synthase can be appreciated in terms of the subunit stoichiometry of $\alpha_3\beta_3\gamma\delta\varepsilon ab_2c_{10-15}$ for the ''simplest'' bacterial form. Much is known about the structure of the enzyme, including high-resolution analyses of the catalytically active F_1-ATPase, as well as its membrane bound counterpart (3–7). Additional studies yielded high-resolution x-ray or NMR models of parts of the enzyme not readily observed in the entire complex, such as the mitochondrial second stalk (8–10), the δ subunit (11), subunit ε (12,13), the bacterial membranous F_0 subunit *c* (14), and part of subunit *b*, including a monomeric transmembrane helix (15) and a monomeric section of the *b* cytosolic domain (16). A low-resolution structure of soluble *Escherichia coli* b_2 and a *b*-δ assembly was recently presented (17). Despite the vast amount of structural information available, significant gaps exist in our overall picture of the enzyme. Not surprisingly, the gaps center on relatively asymmetric structures such as the subunit b_2 bacterial external stalk and heterodimeric cyanobacterial or plant subunit *bb′* external stalk subunits.

Catalysis by ATP synthase uses the electrochemical potential across a membrane to drive rotational movements of a ring of *c*-subunits in the membrane, together with the central-stalk components γ and ε inside the peripherally bound $\alpha_3\beta_3$ ring (1,2). These rotational movements of the internal stalk assembly are thought to drive substrate binding and product release steps in the β subunits in 120° increments (18,19). The external stalk is considered essential to our understanding of the mechanism of ATP synthase because of its putative role in resisting the rotation of the inner core of subunits by linking the peripheral $\alpha_3\beta_3$ ring of catalytic subunits to the membrane-embedded subunit *a*. The membrane domain of subunit *b* was shown to be required for the reconstitution of a functional F_0 sector (20), and the C-terminal end of the *b*-dimer was shown to interact with F_1 via the δ-subunit (21).

A substantial portion of the remainder of the cytoplasmic domain of subunit b_2 was hypothesized to exist in either a dimeric left-handed coiled coil (22,23) or a right-handed dimeric coiled coil with offset helices (16,24). Crick postulated the existence of a left-handed coiled α-helical coil, on the basis of theoretical structural characteristics involving side-chain knobs-into-holes packing interactions that repeat every seven residues as one proceeds along the coil (25). These structures form ''rope-like'' (26) quaternary structures of two, three, or four strands, with repeating heptad positions referred to as *a*, *b*, *c*, *d*, *e*, *f*, and *g*. Left-handed coiled coil structural motifs were found in a great number of proteins (26). The regularity of this motif has lent itself to computational studies that attempted to identify the characteristic coiled coil heptad motif (27–29), and to build model coiled coil molecular structures using either molecular mechanical (30) or simulated annealing (31,32) techniques. The latter approach was applied to modeling the *E. coli* b_2 homodimer (22,23) and the cyanobacterial *bb′* heterodimer (36).

In contrast to the left-handed coiled coil motif, right-handed coiled coils are relatively rare. No known right-handed coiled coils are dimeric. Trimeric and tetrameric right-handed coiled coils are characterized by a shallower

Submitted July 7, 2008, and accepted for publication December 17, 2008.

*Correspondence: jwise@smu.edu

Editor: Mark Girvin.

© 2009 by the Biophysical Society

0006-3495/09/04/2823/9 $2.00

doi: 10.1016/j.bpj.2008.12.3938

pitch than the left-handed versions with 11-residue (undecad) repeats rather than the left-handed heptad repeats (33). Designed peptides with undecad packing motifs were shown in NMR studies to adopt stable trimeric and tetrameric structures, but no evidence of stable right-handed coiled coil dimers was obtained (34). Del Rizzo et al. (24) hypothesized that the *E. coli* subunit *b* dimer adopts a right-handed coiled coil, based on the structural determination of a monomeric form of a 60-residue fragment of the cytoplasmic domain of subunit *b*, the identification of an undecad repeat in the subunit *b* protein sequence, and a series of intermolecular cross-linking studies performed on truncated subunit *b* proteins containing site-specific cysteine substitution mutations (16,24). These studies led Del Rizzo et al. (24) to postulate that the subunit *b* dimer packs in a right-handed dimeric coiled coil structure with an axial offset of four, seven, or 11 amino acids between the residues of each packed helix. Although we presented arguments elsewhere (22,23) for a more conservative interpretation of the cysteine cross-linking experiments of Del Rizzo et al. (24), the hypothesis put forward (24,35) that a right-handed coiled coil can exist with an offset of anything$<$11 residues is difficult to accommodate, because the repeating paired interface packing positions will not mesh properly. In Wood and Dunn (35), for example, a figure depicting such an offset has (among other similar pairs) residues 68 and 72 of one *b* packing with residues 72 and 79 of the second subunit *b*. The putative packing of side chains separated by four residues in one α-helix next to side chains in a second helix that are separated by seven residues (35), while still maintaining an α-helical structure, appears difficult if not impossible to achieve.

Recently, we reported on the modeling of a large portion of the cytosolic regions of both the *E. coli* b_2 (22) and *Synechocystis* bb' (36) dimers as left-handed coiled coils. Both of these structures were validated (23,36) in experiments that combined double site-directed spin labeling (37) within the respective dimers, with distance estimations based on analyses of dipolar interspin interactions as described elsewhere (38–40). The prediction of heptad repeats in the *E. coli* subunit *b* protein (22) indicated that the 11 heptad repeats between residues 31 and 116 are interrupted by two discontinuities known as stutters (41,42). Stutters (three heptad position deletions) are the most common type of discontinuity in heptad repeats (41,43).

Various theoretical considerations led to at least two methods of accommodating stutter discontinuities. Most of this work has focused on homotrimeric or homodimeric coiled coils. Early on, the underwinding of trimeric stuttered coiled coils was observed in influenza hemagglutinin (44–46) and mannose-binding protein (47). Several studies (45,48–50) discussed the global effects of lessening the degree of supercoiling of the helices in coiled coils, and observed that underwinding would loosen the packing of helices, likely resulting in a relative destabilization of the coil. As an alternative to underwinding structures to accommodate stutters, local deformation of folding in the vicinity of the stutter was observed in the dimeric coiled coil of the intermediate filament (45,51,52). This accommodation is predicted to exert little global effect on the coil or its stability.

In a modeling study of the *Synechocystis* bb' dimeric coiled coil external stalk region (36), we described an unusual mismatch in heptad alignments between the monomers, where in a stretch of eight otherwise uninterrupted heptads, one of the monomers had an insertion of four amino acids. This differs from the heptad discontinuity known as a stammer (41), in that in this case the actual length of one of the heterodimeric monomers in this region differed from the other by four amino acids. We were able to model a coiled coil in this region by allowing the inserted residues to loop out of the coil, effectively creating a locally disordered region that accommodated the insert by allowing the heptad matching to continue past the insert region.

In this study, we modeled the *E. coli* subunit *b* dimer with local deformations to accommodate its two heptad stutters, instead of the global underwinding that we previously performed (22). We compared the coiled coil geometries of the two models and validated a new b_2 model, using the interspin distances we measured previously, and by superposition with the high-resolution x-ray structure presented by Del Rizzo et al. (16). Finally, a comparison of the *Synechocystis* bb' and *E. coli* b_2 dimeric coiled coil structures is presented, with a discussion of the apparent functional requirement for destabilizing positions in the external stalk coiled coils of ATP synthases.

MATERIALS AND METHODS

Modeling of locally deformed subunit b_2 external stalk as a left-handed coiled coil

Heptad repeats were predicted using the PAIRCOIL2 program (28). The VMD program (53) and its Tcl/Tk (54) and Python (55) interfaces were used for analyses of protein structures. The cortexillin I structure (56) was used as a basis for b_2 modeling. Interchain and intrachain restraints were based on distances between 12 pairs of Cα atoms and the same set of 12 Cβ atoms (described in 36). Restraint tables were built with these distances as well as φ and ψ dihedrals of 63.7° and 41.7°, respectively, and distances between every tenth and twentieth Cα atoms to 15 and 30 Å (as in Wise and Vogel (22)). Simulated annealing experiments were performed with XPLOR-NIH version 2.18 (57,58), essentially as described previously (22). After the refinement of models based on paired Cα atom distances, paired Cβ distances were added to the restraint set, and the best previous model was used as a template. The refinement of these second iteration models produced the model shown in Fig. 1. Acceptable geometries were defined as having no distance or dihedral restraint violations $>$0.5 Å and 5°, and no bond or improper violation $>$0.05 Å or 5°, respectively. These acceptance values were calculated by XPLOR-NIH for each refined model. The best model was defined as that with the lowest sum of the restraint, angle, dihedral, improper, and bond energies, as calculated by XPLOR-NIH (58). PROCHECK version 3.5 (59) was used to assess the quality of the model shown in Fig. 1. When electron spin resonance (ESR) spectroscopy-determined interspin distances were included, the Protein Data Bank file of the model of Fig. 1 was "mutated," using bash

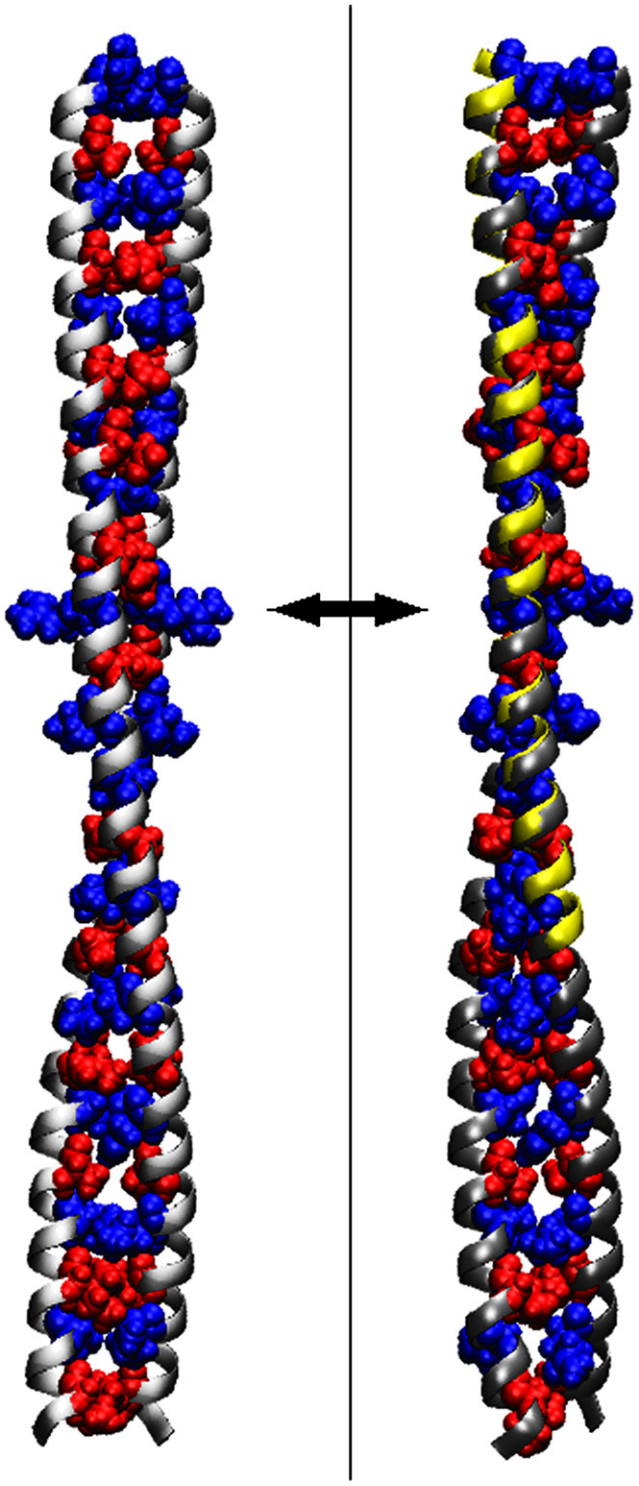

FIGURE 1 Left-handed coiled coil dimerization region of *E. coli* subunit b_2 dimer. (*Left*) Backbone helices of dimerization domain of *E. coli* b_2 are shown in silver, and residues identified as *a* and *d* heptads are shown in space-filling representations in blue or red, respectively. (*Right*) Superposition of monomeric x-ray crystal structure (*yellow backbone*) determined by Del Rizzo et al. (16), with the "A" chain of left-handed coiled coil presented in left panel (*silver backbone*). Heptad *a* and *d* residues are shown in blue and red space-filling representations, respectively. Arrows show position of Arg-83 in the proteins.

scripts to substitute methane thiosulfonate (MTS) spin-labeled cysteinyl residues at appropriate positions. The XPLOR-NIH program, in combination with appropriate topology and parameter files for MTS-cysteinyl residues (22), was then used to build and minimize the residues into the template file. Simulated annealing with the included ESR-determined interspin distance as a restraint, with 10% of the value as an acceptable range, was then performed for each double mutation, as described above. No violation of any distance or angle restraint was evident in any of these MTS-labeled models.

Our computers were Intel Pentium 32-bit single CPU units running Scientific Linux version 5.0 or 5.1. Either 70-CPU or 33-CPU Linux computing clusters, running Scientific Linux version 5.0 or 5.1 operating systems, were used for parallel computation of the model structures.

Determination of knobs-in-holes packing and core-packing angles for coiled coil protein

We employed both the SOCKET program (26) or the theory expressed by Walshaw and Woolfson (26), implemented by us in Tcl scripts for the tkconsole of VMD (53), to determine both the knobs-in-holes center of mass packing and core-packing angles of *a* and *d* knob residues in the ATP synthase external-stalk coiled coil regions.

Molecular modeling of spin-labeled cysteinyl residues

The MTS-spin-labeled cysteinyl residues containing all hydrogens were parameterized, as described by Hornung et al. (23) and Fajer et al. (60).

RESULTS AND DISCUSSION

Local deformations accommodate stutters in *E. coli* subunit *b* dimeric coiled coil

We previously used PAIRCOIL2 (28) to predict repeating coiled coil heptads in the *E. coli* subunit *b* sequence (22). Using a set of known dimeric coiled coils, we then extracted interchain Cα to Cα and Cβ to Cβ distances, as well as φ and ψ angles and long-range Cα to Cα distances, to build restraint tables for use in simulated annealing modeling of the subunit b_2 dimer (22). This modeling procedure produced left-handed dimeric coiled coils that accommodated the two observed stutters in the structure by globally underwinding the coil. More recently, we modeled a 100-residue stretch of *Synechocystis* bb' as a dimeric left-handed coiled coil, and accommodated its discontinuous heptads using local distortions rather than global underwinding. The difference in the two approaches (other than the obvious changes needed to accommodate the heterodimeric nature of the bb' dimer) lay in creating distance restraint tables in the latter case that concentrated primarily on heptad positions known to form knobs (*a* and *d*). These methods were successful in modeling the known left-handed coiled coil dimerization domain of cortexillin I (Protein Data Bank accession number 1D7M) (56) to within a 2-Å root mean-square deviation (RMSD) of backbone atoms over a 100-residue distance (36). Application of these latter methods to the predicted heptads in the *E. coli* subunit *b* sequence (22) (Materials and Methods) resulted in 46 out

of 46 structures with acceptable geometries (Materials and Methods) and no violations of either distance or angle restraints.

Fig. 1 (*left*) shows the best model observed in these studies. Continuous packing of the interface of *a* and *d* residues on the inside surface of the coil is clearly evident. The Arg-83 residue identified as a heptad *a* position (22) shows a lateral ''knobs-across-a-hole'' packing (26) typical of large residues at *a* positions. Despite the three Cβ, Cγ, and Cδ methylene groups, arginines at heptad *a* positions were found to be destabilizing relative to alanine, and to be exclusive to dimeric coiled coil structures (61). PROCHECK (59) analysis of this model indicated 100% core Ramachandran angles, with an overall G-factor of 0.43. SOCKET analysis (26) referred to this structure as a dimeric parallel coiled coil. These results strongly support the hypothesis that the *E. coli* subunit *b* dimer can adopt a left-handed coiled coil structure in the region from residue 31 to 116, and accommodate the two stutters in this region with local deformations instead of global underwinding.

Fig. 1 (*right*) shows the superposition of the ''A'' chain of the left-handed coiled coil and the monomeric crystal structure of the dimerization domain of subunit *b* (16). The average RMSD for heavy backbone atoms in the superposed region for all 46 acceptable structures obtained in this experiment was 0.61 $\pm$ 0.18 SD Å. Similar results were obtained when the x-ray monomer was superposed on the ''B'' chain of the model. In this case, the average RMSD for heavy backbone atoms of all 46 models to the x-ray determined monomer was 0.64 $\pm$ 0.16 SD Å. These results demonstrate that the crystal structure determined for the monomeric subunit *b* protein between residues 62–116 can indeed pack as a left-handed, dimeric coiled coil structure.

Superposition of the monomeric crystal structure (16) on the globally underwound *b*-dimer model reported previously (22) gave an RMSD for heavy backbone atoms of slightly $<$1.5 Å. Comparison of these results with those reported here clearly indicate better overall accommodation of the crystal structure data by the locally deformed model presented in our study (0.6 Å RMSD). Analogous RMSD comparisons of the local regions of stutters with the data of the monomeric crystal structure after superposition of backbone atoms demonstrated that when only the restricted regions of stutters were analyzed on more than 7500 globally underwound and locally deformed *b*-dimer models, no significant differences in lowest RMSD values for the residues in local stutter regions were evident. These RMSD analyses indicate that the locally deformed models, although not significantly better than the globally underwound models at accommodating the monomeric crystal structure data in the limited regions around the two stutters, were much better at predicting the overall structure of the monomeric crystal residues 62–116, as reported by Del Rizzo et al. (16).

Validation of *E. coli* subunit *b* model by interspin distances

We used the model in Fig. 1 for a series of experiments analogous to those presented by Hornung et al. (23) that incorporated double-cysteine mutations in subunit *b*, with corresponding modification of the cysteines with the stable nitroxide spin-label MTS ((1-oxyl-2,2,5,5-tetramethyl-3-pyrroline-3-methyl) methanethiosulfonate). This approach was previously used to test the validity of the modeling of left-handed dimeric coiled coils for subunit *b* that had global underwinding of the coiled coil to accommodate the heptad stutters. In that previous work (23), measurements of interspin distances by ESR were performed on the actual mutated, spin-labeled proteins, and the results were compared with distances obtained for modeled coiled coils.

In our study, we again modeled ESR interspin distances to test the validity of the coiled coil dimer model of subunit *b* that accommodates stutters with local deformations. We used the interspin distances reported by Hornung et al. (23) as additional distance restraints in simulated annealing studies that used all of the restraints and the identical templates that produced the model in Fig. 1. The ESR restraint data were given upper and lower ranges of 10% of the determined values, above which point, restraint violations would occur. The modeling of spin-labeled proteins was performed as described in Materials and Methods.

Fig. 2 reports the results of these experiments. Good correspondence between the modeled and ESR-measured distances was achieved for most of the labeled residues tested. An especially good correlation was evident for measured distances below 25 Å, where the applied continuous-wave ESR technique is reliable. Results for experiments in which the measured ESR distances were too great to be measured with this technique (23) did, in a few cases, result in less optimal fits. We chose 26 Å for the upper limit on continuous-wave ESR interspin distances. Double-labeling at positions 76, 79, 101, and 111 (Fig. 2) showed that in each of these cases, although the 10% range limit was not violated, less optimal solutions were obtained. In these and the remaining 28 experiments, no violations of any restraints and 100% acceptable structures were obtained. In the four cases cited above, no distance or angle restraints were violated, but each of the model structures showed interspin distances that varied from the ESR data by 2–2.5 Å. Visual analysis of the coiled coil regions for these four models gave an impression of a too widely spaced coil that was not as closely packed as in the template structure shown in Fig. 1. The data from these experiments suggest that the subunit *b* coiled coil model calculated here accommodated the ESR interspin data reported by Hornung et al. (23) with great precision, with minor exceptions at those positions (i.e., 75, 79, 101, and 111) that were beyond the detection range of the ESR experiments themselves.

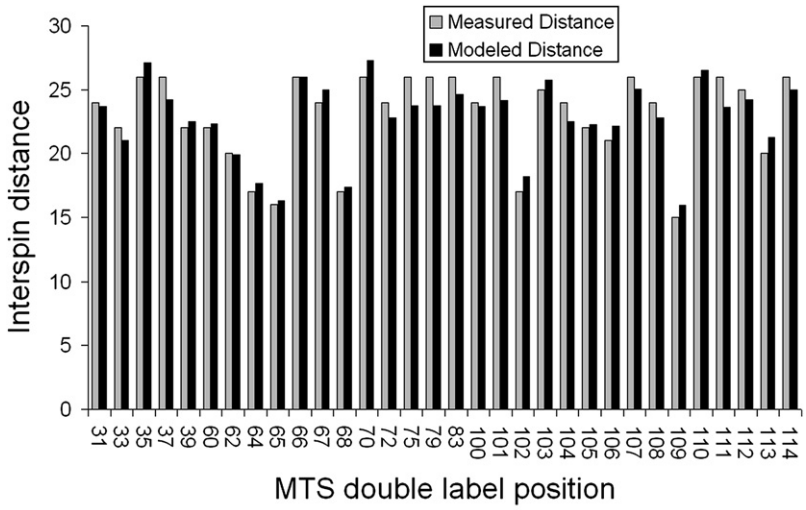

FIGURE 2 Validation of modeled coiled coil with ESR-determined interspin distances. Distances determined for modeled left-handed coiled coils that accommodate stuttered heptads with local deformations are shown in black. Interspin distances that were calculated from ESR measurements made on double spin-labeled subunit *b* proteins, as reported by Hornung et al. (23), are shown in gray.

Lupas and Gruber (62) discussed the global effects of lessening the degree of supercoiling of helices in coiled coils, and predicted that underwinding attributable to the accommodation of stutters would result in the reorientation of the underwound coil in a clockwise rotation, relative to a normally wound coil. This was confirmed here by superposing the N-terminal region of the underwound b_2 structure presented previously (22,23) on the locally deformed b_2 model in Fig. 1 (data not shown).

The coiled coil models presented here, that accommodated the heptad discontinuities with local rather that global deformations, pack significantly tighter than those with global deformations (22,23). This observation is entirely consistent with the theoretical expectations reported by Brown et al. (41) to the effect that one ramification of global deformation to accommodate stuttered heptads is a general loosening of the packing between coiled helices. In addition to these conclusions, one might also speculate that the expected upper limit of detection of interspin distances in the continuous-wave ESR experiments as reported by Hornung et al. (23) should be lowered to <24 Å. For a recent exploration of the limits of continuous-wave and double-electron electron resonance distance measurements, see Banham et al. (63).

Coiled coil "knobs-in-holes" geometries in ATP synthase external stalk models

As summarized elsewhere (26), the packing of coiled coil structures envisaged by Crick (25) has every first and fourth residue of the heptad forming a knob that is packed within a hole created by four residues on another helix. Three of the four ''hole'' residues also function as knobs that complementarily interact with residues that create holes on the original helix. All of this together creates an efficient complementary packing of helices. The ''knobs-into-holes'' packing according to Crick (25) differs from the ''ridges into grooves'' α-helical packing observed in globular proteins (64), in that the former involves the packing of side chains, whereas in the latter, α-carbons form the interface (26,65). The characteristic coiled coil side-chain packing can be very sensitively ascertained by determining the extent to which the knob side chains insert into the side chains that make up the hole. Walshaw and Woolfson published algorithms (26) to quantitate this characteristic by measuring the center of mass of each putative knob-and-hole residue side chain, and determining the extent to which the knobs insert into the holes. We used the SOCKET program of those authors, as well as our own programs, and identified numerous knob-into-hole packing interactions, both in the *E. coli* external stalk b_2 coiled coil model presented here (Fig. 1), and in the underwound external stalk b_2 coiled coil presented by Wise and Vogel (22), as well as the coiled coils for the external stalk of *Synechocystis* synthase (36). SOCKET identified each of these dimers as parallel dimeric coiled coil proteins, as expected (data not shown). Because each of the dimeric left-handed coiled coil models discussed here have *a* and *d* side chains that display rigorous knobs-and-holes packing geometries identified by either the SOCKET program of Walshaw and Woolfson (26) or our own programs (Materials and Methods), these results strongly support our model of *E. coli* b_2 and *Synechocystis* bb' external stalk proteins adopting left-handed coiled coil structures.

Coiled coil core-packing angles in ATP synthase external stalk models

Harbury et al. (66,67), in their studies of mutants of the GCN4 leucine zipper, showed that heptad *a* and *d* side-chain knobs adopt distinct angles between the Cα-Cβ atoms of the knob and the vector between the Cα atoms that makes up the sides of the holes (see Walshaw and Woolfson (26) for a discussion). Those authors showed that the angles can be very characteristic for dimeric, trimeric, and tetrameric coiled coil proteins. In dimeric parallel coiled coils, the ''core-packing

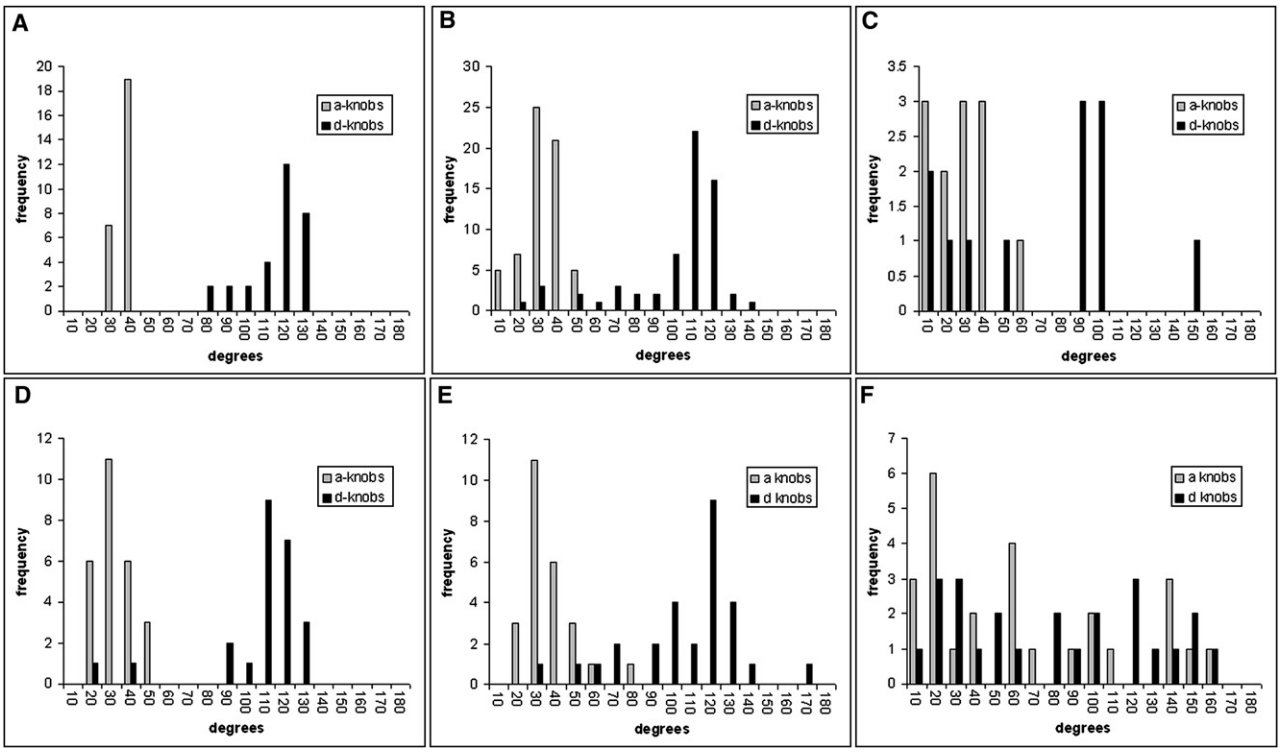

FIGURE 3 Core-packing angles of "a" and "d" knob side chains in crystallographic and modeled coiled coils. Core-packing angles were determined as described in Materials and Methods for three x-ray crystallographically determined dimeric coiled coils and three simulated annealing modeled ATP synthase external stalk coiled coils. (*A*) Perfect coiled coil cortexillin I (1D7M) from Burkhard et al. (56). (*B*) A stuttered coiled coil human vimentin (1GK4) from Strelkov et al. (52). (*C*) Underwound coiled coil from the *E. coli* nucleotide exchange factor, GrpE (1DKG), from Harrison et al. (68). (*D*) Model of b_2 external stalk from *E. coli* ATP synthase (see Fig. 1). (*E*) Model of bb' external stalk from *Synechocystis* ATP synthase (36). (*F*) Underwound model of ATP synthase b_2 external stalk from *E. coli* according to Wise and Vogel (22).

angles'' differ for *d*-layers and *a*-layers, with the *d*-layer inserting between 75° and 125° into the *d*,*e* hole, and in the *a*-layer with angles between 0° and 50° into the *g*,*a* sides of their hole (26). These characteristic angles were observed to flip to their counterparts' angle when antiparallel coiled coil dimers were analyzed (26). Because the side-chain knob-into-hole core-packing angles adopt such very specific geometric relationships, depending on whether the knob is at an *a* or a *d* position, it was of interest to analyze our ATP synthase external stalk models to quantitate these angles.

Fig. 3 presents the core-packing angles of three dimeric coiled coil proteins that were determined by x-ray crystallography (Fig. 3, *A–C*), as well as the angles derived from ATP synthase external stalk coiled coils for *E. coli* b_2 (Fig. 3 *D*), *Synechocystis* bb' (Fig. 3 *E*), and the underwound *E. coli* b_2 presented previously (22). One can see in Fig. 3 that the perfectly repeating heptad motif in cortexillin I (56) (Fig. 3 *A*) gives a very clean separation of *a*-layer and *d*-layer core-packing angles, as does the locally deformed external stalk coiled coil *E. coli* b_2 model presented here (Fig. 3, *D*). Perhaps significantly, the two *d*-knobs that adopted *a*-layer typical angles in Fig. 3 *D* are the two *d*-knobs following the two stutters in subunit *b*. This may reflect the local distortion required for the accommodation of discontinuity in this region. The *Synechocystis* model (Fig. 3, *E*) has core-packing angles for *a* and *d* knobs that are very similar to those determined for the vimentin intermediate filament (52) (Fig. 3 *B*). Interestingly, vimentin has a well documented stutter (45) and also has several *d* knobs with *a*-layer-like angles, whereas the *Synechocystis* model locally compensates for a four-residue insert in one monomer and a single heptad skip (36). Fig. 3 *C* presents core-packing analyses performed on the underwound dimeric coiled coil from the *E. coli* GrpE nucleotide exchange factor (68), and Fig. 3 *F* presents the underwound *E. coli* b_2 model reported previously (22). Both of these proteins accommodate heptad discontinuities in a much more global manner via their underwound coils than was the case for the vimentin, b_2 and bb'structures. These global deformation effects in the GrpE and previously reported b_2 models are apparent in the core-packing angle analyses in Fig. 3, *C* and *F*. The results presented in Fig. 3 show that the locally deformed models for left-handed dimeric subunit *b* coiled coils presented here (Fig. 3 *D*) are much more regular and canonical than are the globally underwound models previously presented (Fig. 3 *F*) (22).

It is clear from the above discussion, and especially from Fig. 3, that the structure of the locally deformed subunit *b*-dimer is much closer to the canonical left-handed coiled

coil structures first envisioned by Crick (25) by virtue of better adherence to canonical core-packing angles and knob-in-hole geometries than is the globally underwound model (compare Fig. 3, *D* and *F*, for example). We hypothesize that this better canonical packing of the locally deformed *b*-dimer model might allow it to function as a stiffer and more elastic stator than a globally underwound model during catalytic turnover by ATP synthase. Increased stiffness and better elastic energy conservation during catalysis by the locally deformed dimer would reflect its presumably lower-energy, more regularly packed, canonical dimer interface, compared with the less ordered, globally underwound model. We suggest that the locally deformed model would be better able to resist unwinding and deformation during catalysis than would the globally underwound model because of its more canonically defined packing interface, or else the locally deformed version would be better able to return any energy invested during catalysis that had unwound or dissociated the dimer interface than would the globally underwound model. The latter alternative would reflect the return of the locally deformed structure in subsequent catalytic substeps to the more maximally stabilized, more defined coiled coil dimer interface, compared with the less well-defined structure of the globally unwound coiled coil. These hypotheses are being tested in molecular dynamics simulations aimed at determining energy differences in dissociation for different *b*-dimer structures.

CONCLUSIONS

It is clear from the side-chain and core-packing analyses shown above that the *E. coli* b_2 external stalk can adopt left-handed coiled coil structures that either locally or more globally accommodate the two stutter discontinuities present in the sequence. The ESR data are not at high enough resolution to distinguish which of the two possibilities is more probable. In addition to these conclusions, it also seems clear that the *Synechocystis* bb' external stalk can also adopt a left-handed coiled coil that accommodates the discontinuities evident in its heterodimeric structure.

It is relevant that Bi et al. (69) recently reported the construction and biochemical analysis of a number of different chimeras between the *E. coli* external stalk b_2 proteins and other coiled coil-forming proteins. Several chimeras between the GCN4 leucine zipper protein and the b_2 proteins did not result in functional external stalks. PAIRCOIL2 analysis of putative heptad repeats showed that at least some of the nonfunctional *b*-GCN4 chimeras created by Bi et al. (69) possessed perfectly repeating heptads throughout the length of the dimerization domain. This leads to the speculation that the coiled coil domain in the *E. coli* external stalk may require the destabilizing influence of heptad discontinuities (such as naturally occurring stutters or nonpairing insertions) to maintain function in ATP synthase. Relevant to this speculation, we recently observed that in the presence of F_1, interspin distances between double spin-labeled cysteine mutants in the region from residues 31–64 in the dimer are significantly farther apart than in the absence of F_1 (Zaida et al., 71). Similar large distances were also observed with five doubly labeled mutants in the same region when complete F_0F_1-ATPase was investigated using double-electron electron resonance spectroscopy (70). Although these residues are N-terminal to the stutters predicted for subunit *b,* it would be interesting if a destabilization of the coiled coil through discontinuity in the packing interface was required for function in ATP synthase.

The authors thank Justin Ross, Joseph Gargiula, Abby Kinney, Allen Hughes, Randall Powell, JoAnn Lan, and James Jaeger of Information Technology Services at Southern Methodist University for the computers used here. Our special gratitude goes to Justin Ross again for his invaluable expertise in setting up and maintaining the computing cluster. The authors also appreciate the help of Ben and Eric Wise in setting up the clusters.

This work was supported by a grant from the National Science Foundation (MCB 0415713) to P.D.V.

REFERENCES

1. Vik, S. 2007. ATP synthesis by oxidative phosphorylation. In EcoSal—*Escherichia coli* and Salmonella: Cellular and Molecular Biology. A. Bock, R. Curtiss III, J.B. Kaper, P.D. Karp, F.C. Neidhardt, T. Nystrom, J.M. Slauch, and C.L. Squires, editors. Available at: http://www.ecosal.org. Accessed October 19, 2007.
2. Weber, J., and A. E. Senior. 2003. ATP synthesis driven by proton transport in F_1F_0-ATP synthase. *FEBS Lett.* 545:61–70.
3. Abrahams, J. P., A. G. Leslie, R. Lutter, and J. E. Walker. 1994. Structure at 2.8 Å resolution of F_1-ATPase from bovine heart mitochondria. *Nature.* 370:621–628.
4. Kabaleeswaran, V., N. Puri, J. E. Walker, A. G. W. Leslie, and D. M. Mueller. 2006. Novel features of the rotary catalytic mechanism revealed in the structure of yeast F1 ATPase. *EMBO J.* 25:5433–5442.
5. Shirakihara, Y., A. G. Leslie, J. P. Abrahams, J. E. Walker, T. Ueda, et al. 1997. The crystal structure of the nucleotide-free alpha 3 beta 3 subcomplex of F1-ATPase from the thermophilic *Bacillus* PS3 is a symmetric trimer. *Structure.* 5:825–836.
6. Stock, D., A. G. Leslie, and J. E. Walker. 1999. Molecular architecture of the rotary motor in ATP synthase. *Science.* 286:1700–1705.
7. Walker, J. E. 1998. ATP synthesis by rotary catalysis. *Angew. Chem. Int. Ed.* 37:2308–2319.
8. Carbajo, R. J., F. A. Kellas, J. Yang, M. J. Runswick, M. G. Montgomery, et al. 2007. How the N-terminal domain of the OSCP subunit of bovine F_1F_0-ATP synthase interacts with the N-terminal region of an alpha subunit. *J. Mol. Biol.* 368:310–318.
9. Carbajo, R. J., J. A. Silvester, M. J. Runswick, J. E. Walker, and D. Neuhaus. 2004. Solution structure of subunit F(6) from the peripheral stalk region of ATP synthase from bovine heart mitochondria. *J. Mol. Biol.* 342:593–603.
10. Dickson, V. K., J. A. Silvester, I. M. Fearnley, A. G. W. Leslie, and J. E. Walker. 2006. On the structure of the stator of the mitochondrial ATP synthase. *EMBO J.* 25:2911–2918.
11. Wilkens, S., S. D. Dunn, J. Chandler, F. W. Dahlquist, and R. A. Capaldi. 1997. Solution structure of the N-terminal domain of the delta subunit of the *E. coli* ATPsynthase. *Nat. Struct. Biol.* 4:198–201.
12. Wilkens, S., and R. A. Capaldi. 1998. Solution structure of the epsilon subunit of the F_1-ATPase from *Escherichia coli* and interactions of this subunit with beta subunits in the complex. *J. Biol. Chem.* 273:26645–26651.

13. Wilkens, S., F. W. Dahlquist, L. P. McIntosh, L. W. Donaldson, and R. A. Capaldi. 1995. Structural features of the epsilon subunit of the *Escherichia coli* ATP synthase determined by NMR spectroscopy. *Nat. Struct. Biol.* 2:961–967.

14. Girvin, M. E., V. K. Rastogi, F. Abildgaard, J. L. Markley, and R. H. Fillingame. 1998. Solution structure of the transmembrane H^+-transporting subunit c of the F_1F_0 ATP synthase. *Biochemistry.* 37:8817–8824.

15. Dmitriev, O., P. C. Jones, W. Jiang, and R. H. Fillingame. 1999. Structure of the membrane domain of subunit *b* of the *Escherichia coli* F_0F_1 ATP synthase. *J. Biol. Chem.* 274:15598–15604.

16. Del Rizzo, P. A., Y. Bi, S. D. Dunn, and B. H. Shilton. 2002. The ''second stalk'' of *Escherichia coli* ATP synthase: structure of the isolated dimerization domain. *Biochemistry.* 41:6875–6884.

17. Priya, R., V. S. Tadwal, M. W. Roessle, S. Gayen, C. Hunke, et al. 2008. Low resolution structure of subunit *b* (*b*22–156) of *Escherichia coli* F_1F_0-ATP synthase in solution and the *b*-delta assembly. *J. Bioenerg. Biomembr.* 40:245–255.

18. Adachi, K., K. Oiwa, T. Nishizaka, S. Furuike, H. Noji, et al. 2007. Coupling of rotation and catalysis in F(1)-ATPase revealed by single-molecule imaging and manipulation. *Cell.* 130:309–321.

19. Boyer, P. D. 1998. ATP synthase—past and future. *Biochim. Biophys. Acta.* 1365:3–9.

20. Greie, J., T. Heitkamp, and K. Altendorf. 2004. The transmembrane domain of subunit *b* of the *Escherichia coli* F1F(0) ATP synthase is sufficient for H(+)-translocating activity together with subunits *a* and *c*. *Eur. J. Biochem.* 271:3036–3042.

21. Rodgers, A. J., S. Wilkens, R. Aggeler, M. B. Morris, S. M. Howitt, et al. 1997. The subunit delta-subunit b domain of the *Escherichia coli* F_1F_0 ATPase. The *B* subunits interact with F_1 as a dimer and through the delta subunit. *J. Biol. Chem.* 272:31058–31064.

22. Wise, J. G., and P. D. Vogel. 2008. Subunit b-dimer of the *Escherichia coli* ATP synthase can form left-handed coiled-coils. *Biophys. J.* 94:5040–5052.

23. Hornung, T., O. A. Volkov, T. M. A. Zaida, S. Delannoy, J. G. Wise, et al. 2008. Structure of the cytosolic part of the subunit *b*-dimer of *Escherichia coli* F_0F_1-ATP synthase. *Biophys. J.* 94:5053–5064.

24. Del Rizzo, P. A., Y. Bi, and S. D. Dunn. 2006. ATP synthase *b* subunit dimerization domain: a right-handed coiled coil with offset helices. *J. Mol. Biol.* 364:735–746.

25. Crick, F. H. C. 1953. The packing of alpha-helices: simple coiled-coils. *Acta Crystallogr.* 6:689–697.

26. Walshaw, J., and D. N. Woolfson. 2001. Socket: a program for identifying and analysing coiled-coil motifs within protein structures. *J. Mol. Biol.* 307:1427–1450.

27. Gruber, M., J. Söding, and A. N. Lupas. 2006. Comparative analysis of coiled-coil prediction methods. *J. Struct. Biol.* 155:140–145.

28. McDonnell, A. V., T. Jiang, A. E. Keating, and B. Berger. 2006. Paircoil2: improved prediction of coiled coils from sequence. *Bioinformatics.* 22:356–358.

29. Wolf, E., P. S. Kim, and B. Berger. 1997. MultiCoil: a program for predicting two- and three-stranded coiled coils. *Protein Sci.* 6:1179–1189.

30. Harbury, P. B., B. Tidor, and P. S. Kim. 1995. Repacking protein cores with backbone freedom: structure prediction for coiled coils. *Proc. Natl. Acad. Sci. USA.* 92:8408–8412.

31. Charest, G., and P. Lavigne. 2006. Simple and versatile restraints for the accurate modeling of alpha-helical coiled-coil structures of multiple strandedness, orientation and composition. *Biopolymers.* 81:202–214.

32. Nilges, M., and A. T. Brünger. 1993. Successful prediction of the coiled coil geometry of the GCN4 leucine zipper domain by simulated annealing: comparison to the x-ray structure. *Proteins.* 15:133–146.

33. Stetefeld, J., M. Jenny, T. Schulthess, R. Landwehr, J. Engel, et al. 2000. Crystal structure of a naturally occurring parallel right-handed coiled coil tetramer. *Nat. Struct. Biol.* 7:772–776.

34. Harbury, P. B., J. J. Plecs, B. Tidor, T. Alber, and P. S. Kim. 1998. High-resolution protein design with backbone freedom. *Science.* 282:1462–1467.

35. Wood, K. S., and S. D. Dunn. 2007. Role of the asymmetry of the homodimeric *b*2 stator stalk in the interaction with the F_1 sector of *Escherichia coli* ATP synthase. *J. Biol. Chem.* 282:31920–31927.

36. Volkov, O. A., T. M. Zaida, P. Voeller, H. Lill, J. G. Wise, and P. D. Vogel. 2009. De-novo modeling and ESR validation of a cyanobacterial F_oF_1-ATP synthase subunit bb′ left-handed coiled coil. *Biochim. Biophys. Acta.* 1787:183–190.

37. Hubbell, W. L., D. S. Cafiso, and C. Altenbach. 2000. Identifying conformational changes with site-directed spin labeling. *Nat. Struct. Biol.* 7:735–739.

38. Hustedt, E. J., R. A. Stein, L. Sethaphong, S. Brandon, Z. Zhou, et al. 2006. Dipolar coupling between nitroxide spin labels: the development and application of a tether-in-a-cone model. *Biophys. J.* 90:340–356.

39. Rabenstein, M. D., and Y. K. Shin. 1995. Determination of the distance between two spin labels attached to a macromolecule. *Proc. Natl. Acad. Sci. USA.* 92:8239–8243.

40. Steinhoff, H. J., N. Radzwill, W. Thevis, V. Lenz, D. Brandenburg, et al. 1997. Determination of interspin distances between spin labels attached to insulin: comparison of electron paramagnetic resonance data with the x-ray structure. *Biophys. J.* 73:3287–3298.

41. Brown, J. H., C. Cohen, and D. A. Parry. 1996. Heptad breaks in alpha-helical coiled coils: stutters and stammers. *Proteins.* 26:134–145.

42. Lupas, A. 1996. Coiled coils: new structures and new functions. *Trends Biochem. Sci.* 21:375–382.

43. Cohen, C., and D. A. Parry. 1990. Alpha-helical coiled coils and bundles: how to design an alpha-helical protein. *Proteins.* 7:1–15.

44. Bullough, P. A., F. M. Hughson, J. J. Skehel, and D. C. Wiley. 1994. Structure of influenza haemagglutinin at the pH of membrane fusion. *Nature.* 371:37–43.

45. Strelkov, S. V., and P. Burkhard. 2002. Analysis of alpha-helical coiled coils with the program TWISTER reveals a structural mechanism for stutter compensation. *J. Struct. Biol.* 137:54–64.

46. Wilson, I. A., J. J. Skehel, and D. C. Wiley. 1981. Structure of the haemagglutinin membrane glycoprotein of influenza virus at 3 Å resolution. *Nature.* 289:366–373.

47. Weis, W. I., and K. Drickamer. 1994. Trimeric structure of a C-type mannose-binding protein. *Structure.* 2:1227–1240.

48. Diez, M., M. Börsch, B. Zimmermann, P. Turina, S. D. Dunn, et al. 2004. Binding of the *b*-subunit in the ATP synthase from *Escherichia coli*. *Biochemistry.* 43:1054–1064.

49. Lupas, A., S. Müller, K. Goldie, A. M. Engel, A. Engel, et al. 1995. Model structure of the Omp alpha rod, a parallel four-stranded coiled coil from the hyperthermophilic eubacterium *Thermotoga maritima*. *J. Mol. Biol.* 248:180–189.

50. Offer, G., M. R. Hicks, and D. N. Woolfson. 2002. Generalized Crick equations for modeling noncanonical coiled coils. *J. Struct. Biol.* 137:41–53.

51. North, A. C., P. M. Steinert, and D. A. Parry. 1994. Coiled-coil stutter and link segments in keratin and other intermediate filament molecules: a computer modeling study. *Proteins.* 20:174–184.

52. Strelkov, S. V., H. Herrmann, N. Geisler, T. Wedig, R. Zimbelmann, et al. 2002. Conserved segments 1A and 2B of the intermediate filament dimer: their atomic structures and role in filament assembly. *EMBO J.* 21:1255–1266.

53. Humphrey, W., A. Dalke, and K. Schulten. 1996. VMD: visual molecular dynamics. *J Mol Graph.* 14:27–28, 33–38.

54. Ousterhout, J. 1994. Tcl and the Tk Toolkit. Addison-Wesley Professional, Upper Saddle River, NJ.

55. Sanner, M. F. 1999. Python: a programming language for software integration and development. *J. Mol. Graph. Model.* 17:57–61.

56. Burkhard, P., R. A. Kammerer, M. O. Steinmetz, G. P. Bourenkov, and U. Aebi. 2000. The coiled-coil trigger site of the rod domain of

cortexillin I unveils a distinct network of interhelical and intrahelical salt bridges. *Structure*. 8:223–230.

57. Nilges, M., J. Kuszewski, and A.T. Brünger. 1991. Sampling properties of simulated annealing and distance geometry. *In* Computational Aspects of the Study of Biological Macromolecules by NMR.J.C. Hoch, F.M. Poulsen, and C. Redfield, editors. Plenum Press, New York. 451–455.
58. Schwieters, C. D., J. J. Kuszewski, N. Tjandra, and G. M. Clore. 2003. The Xplor-NIH NMR molecular structure determination package. *J. Magn. Reson.* 160:65–73.
59. Laskowski, R. A., J. A. Rullmannn, M. W. MacArthur, R. Kaptein, and J. M. Thornton. 1996. AQUA and PROCHECK-NMR: programs for checking the quality of protein structures solved by NMR. *J. Biomol. NMR*. 8:477–486.
60. Sale, K., C. Sár, K. A. Sharp, K. Hideg, and P. G. Fajer. 2002. Structural determination of spin label immobilization and orientation: a Monte Carlo minimization approach. *J. Magn. Reson.* 156:104–112.
61. Wagschal, K., B. Tripet, P. Lavigne, C. Mant, and R. S. Hodges. 1999. The role of position a in determining the stability and oligomerization state of alpha-helical coiled coils: 20 amino acid stability coefficients in the hydrophobic core of proteins. *Protein Sci.* 8:2312–2329.
62. Lupas, A. N., and M. Gruber. 2005. The structure of alpha-helical coiled coils. *Adv. Protein Chem.* 70:37–78.
63. Banham, J. E., C. M. Baker, S. Ceola, I. J. Day, G. H. Grant, et al. 2008. Distance measurements in the borderline region of applicability of CW EPR and DEER: a model study on a homologous series of spin-labelled peptides. *J. Magn. Reson.* 191:202–218.
64. Chothia, C., M. Levitt, and D. Richardson. 1981. Helix to helix packing in proteins. *J. Mol. Biol.* 145:215–250.
65. Efimov, A. V. 1999. Complementary packing of alpha-helices in proteins. *FEBS Lett.* 463:3–6.
66. Harbury, P. B., P. S. Kim, and T. Alber. 1994. Crystal structure of an isoleucine-zipper trimer. *Nature*. 371:80–83.
67. Harbury, P. B., T. Zhang, P. S. Kim, and T. Alber. 1993. A switch between two-, three-, and four-stranded coiled coils in GCN4 leucine zipper mutants. *Science*. 262:1401–1407.
68. Harrison, C. J., M. Hayer-Hartl, M. Di Liberto, F. Hartl, and J. Kuriyan. 1997. Crystal structure of the nucleotide exchange factor GrpE bound to the ATPase domain of the molecular chaperone DnaK. *Science*. 276:431–435.
69. Bi, Y., J. C. Watts, P. K. Bamford, L. K. Briere, and S. D. Dunn. 2008. Probing the functional tolerance of the *b* subunit of *Escherichia coli* ATP synthase for sequence manipulation through a chimera approach. *Biochim. Biophys. Acta*. 1777:583–591.
70. Steigmiller, S., M. Börsch, P. Gräber, and M. Huber. 2005. Distances between the *b*-subunits in the tether domain of F_0F_1-ATP synthase from *E. coli*. *Biochim. Biophys. Acta*. 1708:143–153.
71. Zaida, T. M., T. Hornung, O. A. Volkov, A. D. Hoffman, S. J. Pandey, J. G. Wise, and P. D. Vogel. 2008. Conformational changes in the *Escherichia coli* ATP synthase b-dimer upon binding to F_1-ATPase. *J. Bioenerg. Biomembr.* 40:551–559.